Satellite-based estimation of actual evapotranspiration in the Buyuk Menderes Basin, Turkey

Hakan Aksu and Alparslan Arikan

ABSTRACT

Evapotranspiration (*ET*) is one of the most important components of the hydrological cycle, but it is often the most difficult variable to determine at basin scale. Traditionally, *ET* is estimated using point-based measurements collected at meteorological stations, but the non-spatial nature of these measurements often leads to significant errors when utilized at watershed scale. In this study, the METRIC (mapping evapotranspiration at high resolution with internalized calibration) approach was evaluated using remotely sensed observations from the moderate resolution imaging spectroradiometer sensor and data from meteorological stations in the lower catchment of the Buyuk Menderes Basin in western Turkey in the form of actual *ET* maps at daily and monthly intervals between 1st April and 30th September 2010. The energy fluxes and daily *ET* maps resulting from METRIC were compared with *ET* data estimated with the help of meteorological parameters. These results were found to be compatible with the ground-based estimations which suggest considerable potential for the METRIC model for estimating spatially distributed actual *ET* values with little ground-based weather data.

Key words | energy balance, *ET*, METRIC, MODIS, remote sensing

Hakan Aksu (corresponding author)
State Hydraulic Works of Turkey,
No. 16 06100,
Çankaya,
Ankara,
Turkey
E-mail: *hakana@dsi.gov.tr*

Alparslan Arikan
Hacettepe University Hydrogeology Engineering Department,
Beytepe,
Ankara 06800,
Turkey

INTRODUCTION

Evapotranspiration (*ET*) is an important component of the Earth's water and energy cycles. For example, average annual evapotranspiration from the global land surface is around 60 to 65% of precipitation (Baumgartner & Reichel 1975). Estimation of actual *ET* is also crucial for hydrologic modeling, water and irrigation planning, management, drought assessment, water rights, aquifer recharge assessment, and many other areas. One of the main parameters for the determination of water needs for irrigation is actual *ET*. For this reason, estimation of actual *ET* provides very valuable information for the effective management of irrigation. Evapotranspiration is also crucial for the energy cycle. More than half of the solar energy absorbed by land surfaces is currently used to evaporate water (Trenberth *et al.* 2009), significantly affecting the Earth's climate.

The methods for estimating basin-wide *ET* are generally grouped into three categories: the water budget approach, meteorological estimate, and remote sensing of the land–atmosphere interface. Hydrological methods such as Thornthwaite & Matter (1955) and Grindley (1969) utilize an accounting approach where inflow, outflow, and change in storage are used in the water budget. Meteorological methods are based mainly on temperature and radiation data. Formulations proposed by Turc (1961) and Thornthwaite (1948) are commonly used by hydrology practitioners. Agro-meteorological methods use potential *ET* data as a reference, and crop coefficients are multiplied according to crop type and crop stage (Penman 1948). Remote sensing-based *ET* methods utilize the energy budget concept and generally provide accurate and spatially explicit estimates of *ET* (Allen *et al.* 2005).

The first two methods can be identified as conventional techniques and use point-based hydrometeorological data. However, with proper adaptations to use remote sensing

doi: 10.2166/nh.2016.226

data, conventional methods such as Monteith (1965) and Priestley & Taylor (1972) are also widely applied in a spatially distributed manner (e.g., Vinukollu *et al.* (2011), Miralles *et al.* (2011), among others). The spatial variation of the parameters affecting the *ET* process is so high that uncertainty increases with the increasing scale of hydrological basins. To this end, remote sensing techniques provide large and continuous spatial coverage and are applicable especially for large areas. Moreover, remote sensing techniques are advantageous over point-based methods for estimating *ET* from crop coefficients or vegetation indices in that neither crop development stages nor specific crop types need to be known (Allen *et al.* 2011). The use of remote sensing data in *ET* models (both conventional or energy balance models) enables the spatial distribution of *ET* over large areas.

Remote sensing-based *ET* algorithms are based on the rationale where available energy in the environment is used for the vaporization process (Su 2002). Along with other surface parameters such as leaf area index (*LAI*), surface albedo, surface emissivity and radiometric surface temperature – also derived from remote sensing – and surface meteorological variables, remote sensing algorithms are capable of estimating *ET* on local, regional, and global scales. Generally known as the energy budget methods, these algorithms use physical and empirical relations together to estimate *ET* as the residual of the land surface energy budget equation. There are many models based on residual methods, such as SEBAL (Bastiaanssen *et al.* 1998a, 1998b), SEBI (Menenti & Choudhury 1993), SEBS (Su 2002), mapping evapotranspiration at high resolution with internalized calibration (METRIC) (Allen *et al.* 2007a, 2007b), and S-SEBI (Roerink *et al.* 2000).

Many studies have tested the performance of the METRIC model at various scales. Gowda *et al.* (2008) evaluated the performance of the METRIC model in Texas plains using Landsat 5 TM data and found good correlation with ET estimations based on the soil water budget model. Choi *et al.* (2009) conducted a comparison of the two-source energy balance (TSEB) model, METRIC, trapezoid interpolation model, METRIC, and TSEB models, and consequently, found relatively good agreement between models for *Rn* and *G* but greater disagreement for *H* and *LE* between models and also among the observation data. Gonzalez-Dugo *et al.* (2009) compared METRIC and TSM models and underlined the requirement of models for accurate surface temperature input. Singh & Senay (2016) found that estimated daily ET for both cropland and grassland had some degree of linearity with METRIC, SEBAL, and SEBS. Paul *et al.* (2013) showed the sensitivity of SEBAL to excess resistance to heat transfer parameter (kB-1). Paul *et al.* (2014) underlined the importance of hot and cold pixel selection, and proposed spatial and temporal adoption of kB-1 variable for better model performance. *ET* models have strengths and limitations for applications in water resource management. In this study, we used the METRIC algorithm to calculate *ET* using moderate resolution imaging spectroradiometer (MODIS) remotely sensed images and ground-based meteorological observations on cloud-free days. METRIC is a variant of SEBAL, which incorporates autocalibration procedures by ground-based reference *ET* and uses evaporative fraction to extrapolate *ET* in image time to daily scales in order to lessen regional advection differences (Allen *et al.* 2011). In the study hourly, daily, and monthly values of *ET* were calculated for the study area. Further, the effect of spatio-temporal change on the *ET* values was evaluated. Intercomparison of the model results was made by *ET* values calculated by the Penman–Monteith equation ASCE version in an experimental area covered with olive orchards in the study area. The main objective of this study was to assess the capability of remote sensing-based *ET* estimation via the METRIC model in the lower part of the Buyuk Menderes River Basin in western Turkey. The *ET* maps produced as outputs are planned to be used in the assessment of irrigation planning studies.

STUDY AREA

The Buyuk Menderes River, which is the largest river of the Aegean region of Turkey, has a length of 584 km and a drainage area of 24,873 km^2. The downstream part of the basin was chosen as the study area, which includes the Soke Plain in Aydın province. The study area lies between 37.36 °–38.06 ° N and 27.03 °–27.93 °E and covers an area of 3,560 km^2 (Figure 1). The altitude increases from west to east. The study area is an important irrigation area for

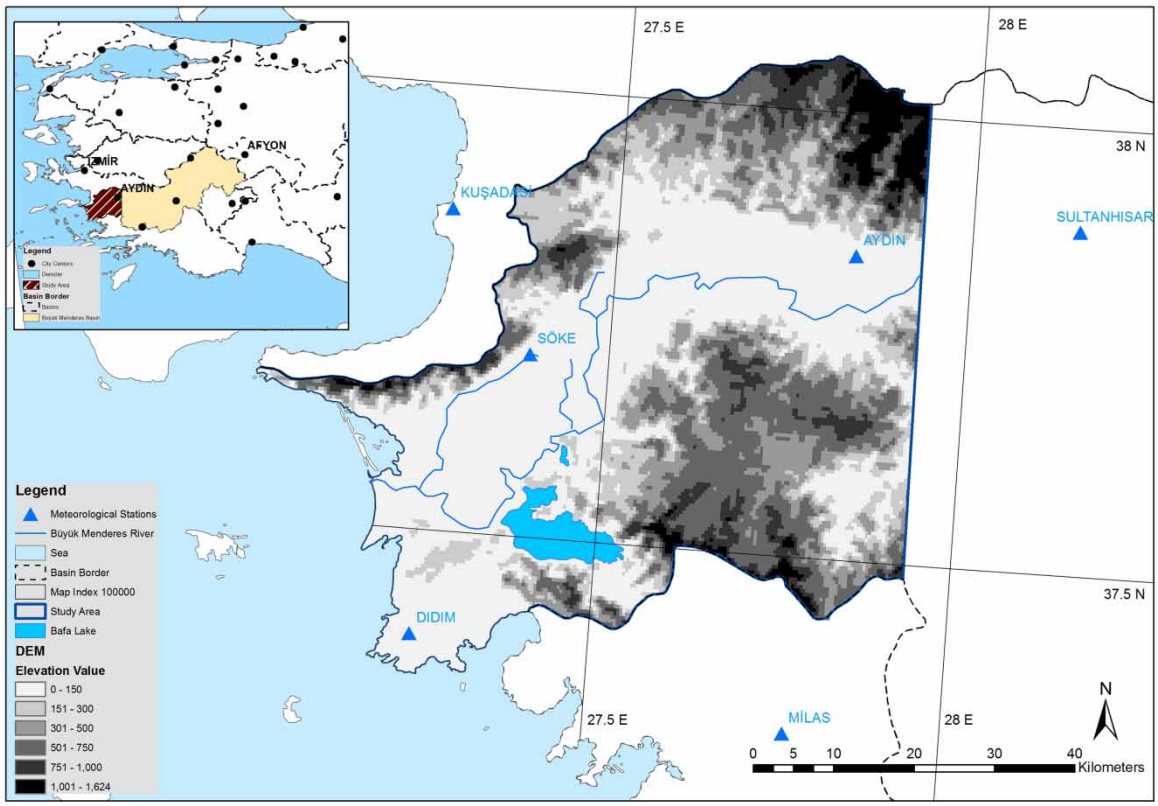

Figure 1 | Location of study area and meteorological stations.

Turkey, and cotton is the primary irrigated crop. Therefore, the study period was chosen from the beginning of the cultivation (irrigation) to the end of the cotton harvest in the lower part of Buyuk Menderes Basin. The chosen study area only includes the lower plain of the Buyuk Menderes Basin so as to exclude the uncertainties resulting from high elevation and aspect effects. Annual average, monthly minimum, and maximum temperatures are 17.6 °C, 8.1 °C, and 30.7 °C, respectively. The long-term average annual total precipitation and pan evaporation values are 627 mm and 1,378 mm, respectively.

METHODOLOGY

Data

Meteorological data required by the surface energy balance model include minimum, maximum, and average temperatures, actual vapor pressure, pan evaporation (class A-pan), wind speed, air temperature, and cloudiness. The data are based on hourly and daily time scales. In this study, the observations from six meteorological stations located in and around the study area were used.

Remotely sensed data were obtained from MODIS products (see details in Table 1) because it provides surface observations for regional/basin water management. MODIS is the key instrument aboard the Aqua and Terra

Table 1 | MODIS products

MODIS standard products	Parameter	Spatial resolution	Temporal resolution
MOD13A2	Vegetation indices (*NDVI*)	1,000 m	16 days
MOD15A2	Leaf area index (*LAI*)	1,000 m	8 days
MOD11A1	Land surface temperature and emissivity	1,000 m	Daily
MOD09GA	Surface reflectance	1,000 m	Daily
MOD35L2	Cloud mask	1,000 m	Daily

satellites, acquiring data in 36 spectral bands. The primary remotely sensed inputs to the METRIC algorithm are normalized difference vegetation index (*NDVI*), surface emissivity, broadband surface albedo, and land surface temperature. The MODIS albedo is calculated as (Liang 2001):

$$\alpha = 0.160r_1 + 0.291r_2 + 0.243r_3 + 0.116r_4 + 0.112r_5 + 0.081r_7 - 0.0015 \quad (1)$$

where α is the broadband albedo and r_n represents spectral reflectance in band n.

Since clouds have negative effects on the detection of reflectivity from the Earth's surface, cloud-free days for the study area were determined by the evaluation of the cloudiness data obtained from meteorological stations for the satellite passing times as well as with the help of the MODIS cloud mask product.

The MODIS Reprojection Tool was used to reproject the coordinate system to *UTM* with *WGS 84* Datum. COoRdination of INformation on the Environment (CORINE) land cover data set of the year 2006 was used to determine the surface roughness for momentum transport (Figure 2).

Model description

The METRIC model is a satellite image processing model which estimates *ET* as a residual of energy balance for the time of sensor overpass (Choudhury 1994; Allen *et al.* 2007a, 2007b; 2011) considering the following equation:

$$LE = Rn - G - H \quad (2)$$

where $Rn\ (W/m^2)$ is the net radiation, $G\ (W/m^2)$ is the ground (soil) heat flux, $H\ (W/m^2)$ is the turbulent sensible heat flux, and LE (W/m^2) is the turbulent latent heat flux (energy equivalent of *ET*). The net radiation flux is the difference between downward and upward radiation fluxes at the

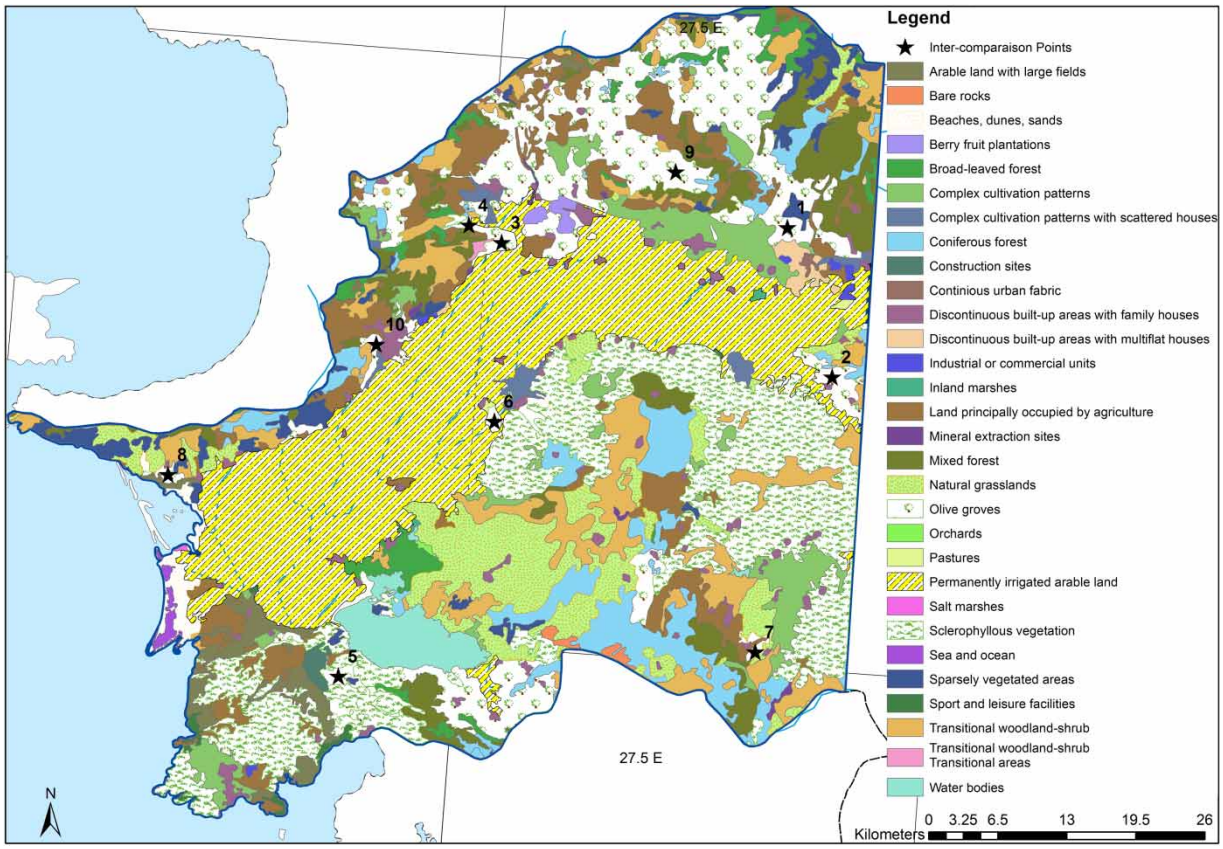

Figure 2 | Inter-comparison points shown on CORINE map.

land surface both in shortwave and longwave parts of the spectrum, and calculated as:

$$Rn = RS\downarrow - \alpha\, RS\downarrow + RL\downarrow - RL\uparrow - (1-\varepsilon_o)RL\downarrow \quad (3)$$

where $RS\downarrow$ is downward solar radiation (W/m^2), α is land surface albedo, $RL\downarrow$ is downward longwave radiation (W/m^2), $RL\uparrow$ is upward longwave radiation (W/m^2), and ϵ_o is emissivity of the surface (–).

$R_{s\downarrow}$ is calculated assuming clear-sky conditions as a constant for image time using Equation (4):

$$R_{s\downarrow} = G_{sc} \times \cos\ \theta \times d_r \times \tau_{sw} \quad (4)$$

where G_{sc} is the solar constant (1,367 W/m^2), cos θ is the cosine of the solar incidence angle, d_r is the inverse squared relative earth–sun distance, and τ_{sw} is the atmospheric transmissivity. τ_{sw} is obtained from Equation (5) (Allen *et al.* 1998):

$$\tau_{sw} = 0.75 + 2\times10^{-5}\times z \quad (5)$$

where z is the elevation above sea level (m).

$R_{L\downarrow}$ is computed using the Stefan–Boltzman equation:

$$R_{L\downarrow} = \varepsilon_a \times \sigma \times T_a^4 \quad (6)$$

where ε_a is the atmospheric transmissivity (dimensionless), σ is the Stefan–Boltzman constant (5.67×10^{-8} W/m^2/K^4), and T_a is the near surface air temperature (°K). The following empirical equation for ε_a by Bastiaanssen (1995) was applied:

$$\varepsilon_a = 0.85 \times (-\ln\ \tau sw) \quad (7)$$

$RL\uparrow$ is also calculated by the Stefan–Boltzman equation:

$$R_{L\uparrow} = \varepsilon_o \times \sigma \times T_s^4 \quad (8)$$

where ε_o is the broad-band surface emissivity (dimensionless) and T_s is the surface temperature (^oK).

Soil heat flux is defined as the rate of heat flow into the soil due to conduction. Soil heat flux (G) was modeled as a function of Rn, vegetation index, surface temperature, and surface albedo near midday values (Bastiaansen 1995) as given by:

$$\frac{G}{Rn} = \frac{Ts}{\alpha}\left(0.0038\,\alpha + 0.0074\alpha^2\right)*\left(1 - 0.98\ \mathrm{NDVI}^4\right) \quad (9)$$

where T_s is surface temperature (°K).

Calculation of the sensible heat flux (H) is performed by using the bulk aerodynamic resistance method:

$$H = \frac{\left(\rho_a \times C_p \times dT\right)}{r_{ah}} \quad (10)$$

where ρ_a is the density of moist air (kg/m^3), C_p is specific heat capacity of dry air (~1,004 J/kg.K), T is the average air temperature (°K) at screen height (typically at 2 m), dT is the near surface temperature difference between two levels (°K K), which are 2 m and 0.1 m (Allen *et al.* 2011), and r_{ah} is the aerodynamic resistance to heat transfer (s/m).

In METRIC, the momentum roughness length (z_{om}) is estimated for each pixel based on land use type. Brutsaert (1982) and Allen (1996) defined the general values for different land use types. In agricultural areas, a relationship proposed by Tasumi (2003) is used:

$$z_{om} = 0.018 \times \mathrm{LAI} \quad (11)$$

$$dT = a + b \times T_s \quad (12)$$

The key to METRIC is to determine the a and b constants using the hot pixel (T_s is high due to no evapotranspiration) and cold pixel (low surface temperature because of the evaporative cooling) which were identified with the help of visual image interpretation, and sensible heat flux values were calculated for hot and cold pixels. This value is corrected for atmospheric stability, which involves an iterative process using the Monin–Obhukov similarity theory. H values are converted to dT_{hot} and dT_{cold} values, and then a line is fitted through the pair of T_s and dT values to determine a and b values.

The instantaneous LE is obtained using Equation (2), and then it is converted to Et_{inst}:

$$ET_{inst} = 3600 \times \lambda ET \quad (13)$$

Table 2 | Processed image dates

Date (year: 2010)	Julian days	Date	Julian days
23 April	113	14 July	195
3 May	123	2 August	214
14 May	134	17 August	229
30 May	150	29 August	241
15 June	166	11 September	254
2 July	183		

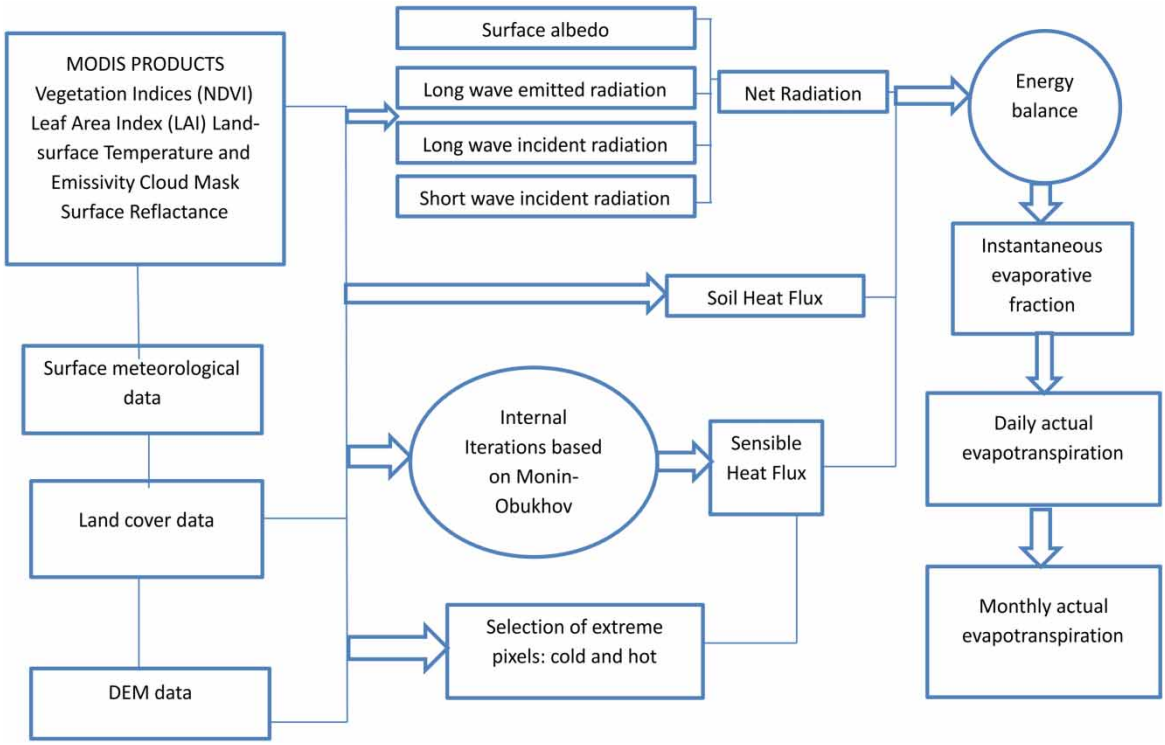

Figure 3 | Flowchart of ET estimation by using METRIC.

where ET_{inst} is hourly actual evapotranspiration (mm/hr), and λ is latent heat flux (J/Kg).

METRIC uses the fraction of alfalfa reference *ET (ETrF)* to obtain the daily *ET* from instantaneous observations. This is the ratio of the actual crop *ET* to *ETr* at the time of overpass, and it is also assumed to be constant throughout the day:

$$ETrF = \frac{ET_{inst}}{ETr} \tag{14}$$

where *ETr* is alfalfa reference evapotranspiration (mm/hr).

Therefore, the daily *ET* is obtained by multiplying *ETrF* by *ETr-24*; the latter being *ETr* for the day, obtained by summing hourly reference *ET* for the entire day. This approach is capable of capturing most of the advection impacts and any other change in weather conditions during the day.

$$ET24 = ETrF \times ETr24 \tag{15}$$

The METRIC approach assumes that the *ET* for the entire area of interest changes in line with *ETr* calculated for the

Table 3 | Crop coefficients for olive orchard (Pastor & Orgaz 1994)

Months	*Kc* coefficients	Months	*Kc* coefficients
January	0.5	July	0.45
February	0.5	August	0.45
March	0.65	September	0.55
April	0.60	October	0.60
May	0.55	November	0.65
June	0.50	December	0.50

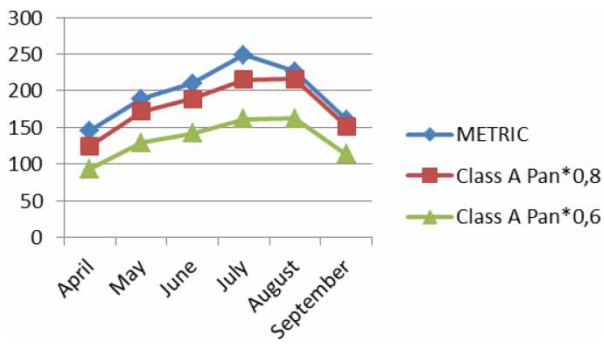

Figure 4 | Bafa Lake monthly total evaporation and pan evaporation (mm).

representative weather station (Allen *et al.* 2007a, 2007b). Estimation of *ET* for non-processed image days (whether cloudy or clear sky) by using clear-sky processed satellite image data is an effective approach (Tasumi *et al.* 2005). Generally, one satellite image per month is sufficient to construct an accurate *ETrF* curve for estimating seasonal *ET*. However, more frequent image intervals are needed in periods of rapid vegetation growth. In this study, the intervals of images were chosen as 10 to 20 days for better representation of all vegetation growth period in the study area (Table 2).

Monthly ET is calculated as:

$$ETm = \sum_{i=1}^{m}[(ETrFi)(ETr24i)] \quad (16)$$

where *ETm* is cumulative *ET* for a month ending on day m, *EtrFi* is interpolated *ETrF* for day *i*, and *ETr24i* is 24-h *ETr* for day *i*. Units are in mm day^{-1}.

In this research, the scheme for estimation of *ET* by METRIC is based on MODIS products and is given in Figure 3.

As there is no direct measurement of *ET* over the study area, the method used by Jia *et al.* (2009) in the case of the Yellow River Basin in China was used for the inter-comparison process. Jia *et al.* (2009) proposed an alternative method to make comparisons with modeled and observed data. In their method, *ET* was estimated by multiplying the reference *ET* derived from the Penman–Monteith equation by the crop coefficients. In this study, reference evaporation estimation calculated by the Penman–Monteith ASCE version was used to make comparison with the METRIC *ET* outputs. Converting the reference *ET* to actual *ET* was made by the crop coefficient for olive trees. Pastor & Orgaz (1994) determined the crop coefficient (*Kc*) values of olive trees on a monthly basis for the area, 60% of which is covered with olive trees (Table 3). For inter-comparison purposes, 10 points covered with olive trees in the study area were chosen.

Bafa Lake, located in the study area, was selected for the estimation of evaporation from water surfaces such as lakes and reservoirs. Class A-pan evaporation measurements at

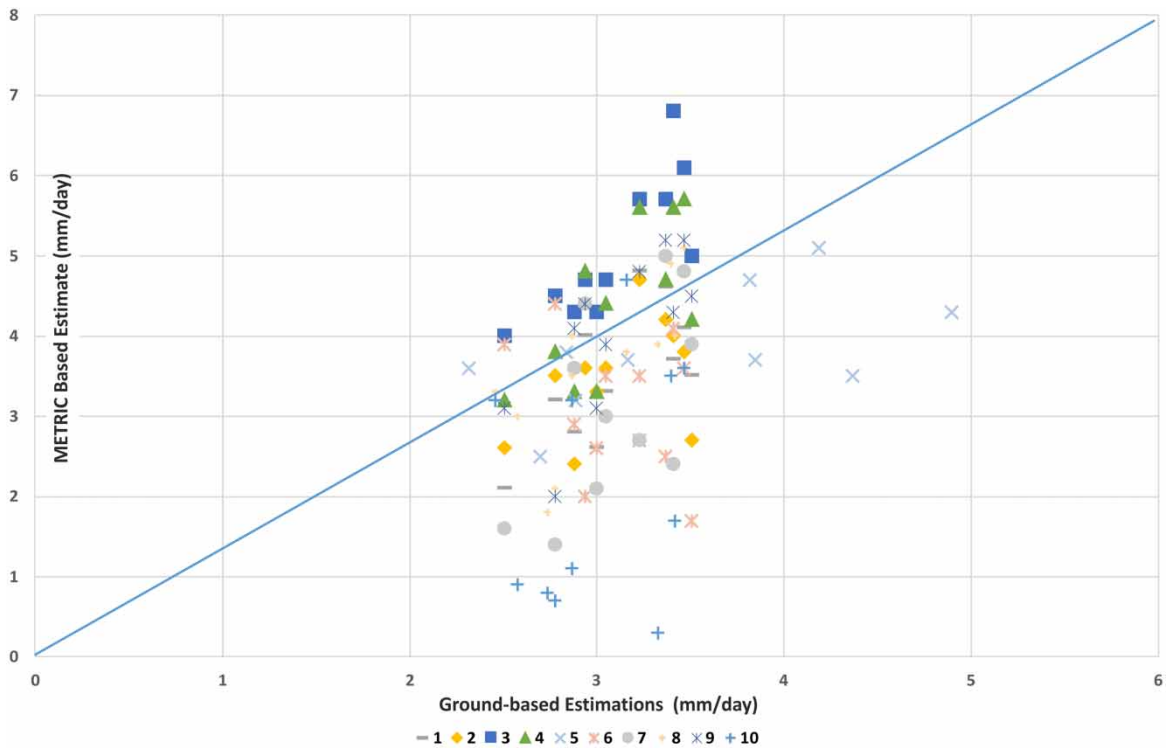

Figure 5 | Comparision between METRIC and ground-based estimations for inter-comparison points (1:1 scale).

Kusadasi Station were used to compare Bafa Lake evaporation estimations by METRIC. Class A-pan conversion coefficients ranged between 0.6 and 0.8 (WMO 2008). Class A-pan measurements multiplied with different pan coefficients ranged between 0.6 and 0.8, and METRIC and pan estimations are presented in Figure 4. When combined with an appropriate pan coefficient or with an adjustment for the energy exchange through the sides and bottom of the tank, evaporation data from a Class-A pan can be considered to be open-water evaporation (Dingman 1992).

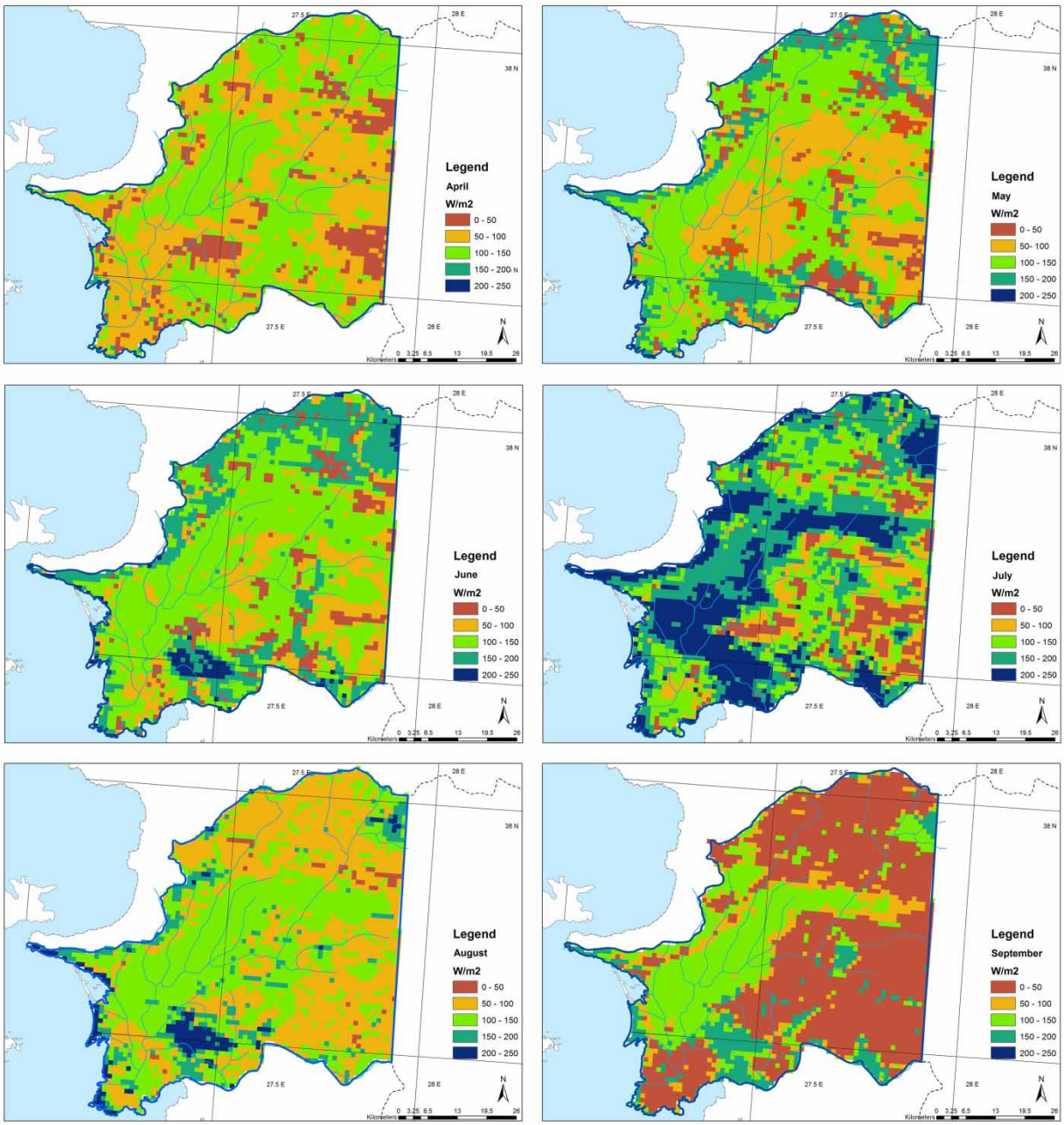

Figure 6 | Monthly total ET (in mm/month) from April to September.

RESULTS AND DISCUSSION

In this study, a remote sensing algorithm, METRIC, was applied to estimate basin-wide actual *ET* in the lower part of the Buyuk Menderes Basin in Western Turkey. The spatial distribution of actual evapotranspiration for the cotton growing season was mapped at daily and monthly time steps. The model results were validated by comparing remote sensing estimates to ground-based actual *ET* estimations calculated with the help of the Penman–Monteith equation adjusted by coefficients on olive orchards.

The average standard error in daily *ET* estimates for the processed 11 imagery is 16.1%, and standard deviation is 27.1% (Figure 5). When compared to results of a similar study conducted under similar climatic conditions, Allen (2014) found METRIC to have 1.6% minimum bias in an application for an agricultural area equipped with flux measurements. In our work, the maximum differences were found at points 3 and 4, which also correspond to locations with the maximum slope values (24.8% and 24.0%, respectively). The mean and standard deviation of slopes in all points are 11.5% and 7.5%, respectively. Therefore, the deviation between METRIC and ground-based *ET* estimates appears to be associated with the ground slope. However, the METRIC's slope-correction ability was not used in this study since the cotton fields are almost flat. In addition to high slope areas, another reason for the less than ideal bias in our work is related to the nature of limited data used in the Penman–Monteith equation.

Average monthly actual *ET* during the cotton growing season in the lower part of the Buyuk Menderes Plain

Table 4 | Land use and monthly ET

Land cover type	Area (km^2)	Months	Total ET (mm)	Mean (mm)	Standard deviation
Agricultural lands	1,757.7	April	176,064.0	95.9	26.8
		May	209,312.1	113.8	33.1
		June	232,404.6	126.0	32.2
		July	302,526.2	162.5	48.6
		August	196,126.0	104.8	32.0
		September	111,855.3	84.9	44.4
Forest and semi-natural lands	1,615.8	April	148,655.0	90.4	35.5
		May	167,255.9	102.9	46.2
		June	188,299.9	114.2	49.1
		July	218,578.0	132.8	66.9
		August	198,516.7	114.6	42.8
		September	105,428.0	65.7	53.4
Wetlands	3.1	April	229.6	57.5	37.3
		May	248.5	62.1	40.4
		June	414.4	103.6	20.0
		July	758.9	189.7	25.0
		August	663.8	166.0	21.1
		September	482.2	120.6	38.9
Water bodies	75.7	April	12,108.4	126.1	32.1
		May	15,966.6	164.6	47.5
		June	17,782.5	183.3	40.0
		July	22,385.3	228.4	40.0
		August	18,510.4	210.3	38.8
		September	14,140.2	148.8	31.5
Artificial areas	105.1	April	10,257.7	71.2	39.0
		May	13,441.4	87.3	50.1
		June	14.822.3	98.2	50.5
		July	18,145.3	121.8	58.5
		August	16,301.7	91.1	37.5
		September	6,844.1	54.8	45.7

ranges from 99.6 mm in April to 194.3 mm in July, whereas maximum and minimum monthly actual *ET* were estimated as 240.7 mm in July and 37.2 mm in April for the entire study area. To this end, the temporal and spatial details of *ET* maps afforded by the METRIC model are significant especially when compared to estimation by point-based measurements that can cause substantial errors (Figure 6).

The major land cover types in the study area are agriculture (50%), forest and semi-natural lands (46%), the remainder being water and wetlands (3%) and artificial areas (1%). It was found that open water bodies have the highest *ET* values followed by agricultural areas due to large-scale irrigation. The areas of the land cover categories and the corresponding amount of water consumption

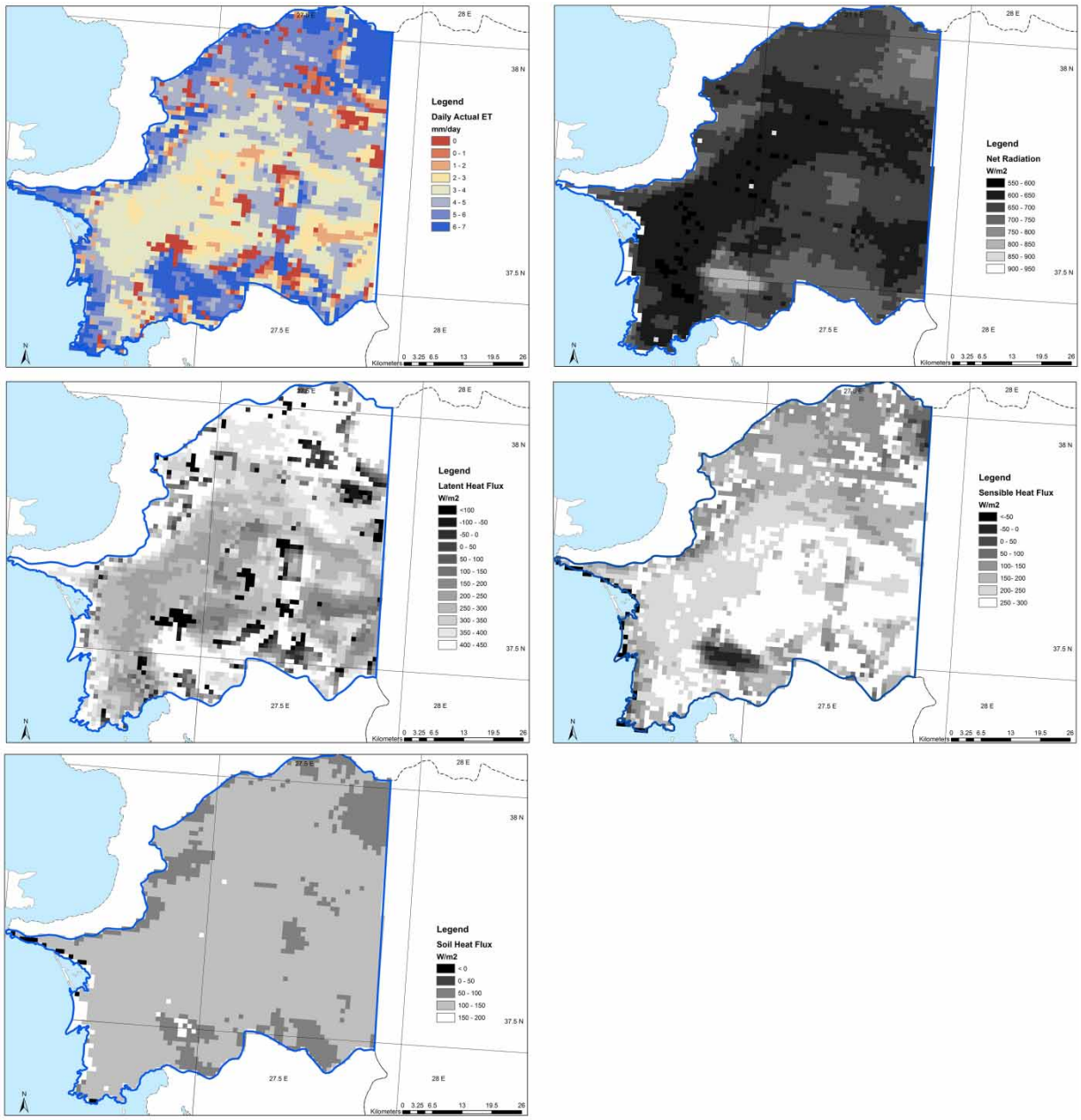

Figure 7 | Daily actual evapotranspiration and energy balance components (15 June 2010).

estimated in this study are given in Table 4. As shown, the water consumption in the study area is dominated by agricultural and forest/semi-natural lands which cover the majority of the landscape (94.8%), and the *ET* rate of these areas accounts for over 92% of total consumption during the study period. Agricultural lands (49.4%) have the highest consumption (50.4%) as regards to the integrated impact of land coverage on the ET rate.

Bafa Lake daily evaporation rates were estimated with 16.4% average standard error and 15.0% standard deviation for the 11 processed images. These results are compatible with Class-A pan-based lake evaporation rates. Monthly evaporation on Bafa Lake ranged between 145.4 mm in April 2010 and 248.7 mm in July 2010.

In addition to the spatial and temporal distribution of *ET*, energy balance components were also determined (Figure 7). The produced data on energy balance components can be a tool for further analysis such as comparison of available energy for evapotranspiration and measured *ET* values.

CONCLUSIONS

In this study, the use of remote sensing along with ground-based data to determine *ET* at a regional scale is demonstrated, and promising results are achieved. The spatial and temporal variation of *ET* was found to be significant due to the land use, meteorological conditions, and vegetation patterns. METRIC evaporations are in agreement with the Class A-pan data. As the METRIC *ET* estimations are closely aligned with the Class A-pan data, the method can also be used for estimating evaporation from lakes in data-scarce areas. Remote sensing-based pan coefficients can also be developed for monitoring of lakes.

The gridded *ET* maps can be used as input for hydrological models. They also have the potential to increase the effectiveness of water management strategies by determining irrigation requirements in spatially explicit ways. Moreover, spatially distributed evapotranspiration data on cultivated lands can be used to calculate crop water productivity (kg/m^3), which is a powerful tool to assess the efficiency of different irrigation management systems including structural and non-structural applications such as irrigation schemes and legal and institutional frameworks.

This study forms a basis for estimation of *ET* for regional-scale applications particularly over agricultural areas in western Turkey. Future studies should include other *ET* models based on remote sensing data to determine the efficiency of respective models under the climate regime of western Turkey.

ACKNOWLEDGEMENTS

The authors thank their colleagues Dr S. Bayari and Dr A.U. Sorman for continuing support and discussions during this study.

REFERENCES

Allen, R. G. 1996 Assessing integrity of weather data for reference evapotranspiration estimation. *J. Irrig. Drain. Eng.* **122** (2), 97–106.

Allen, R. G. 2014 Ecostress METRIC evapotranspiration algorithm. In: *HyspIRI Science and Application Workshop*, 14–16 October, Pasadena, CA, USA.

Allen, R. G., Pereira, L. S., Raes, D. & Smith, M. 1998 *Crop Evapotranspiration – Guidelines for Computing Crop Water Requirements*. FAO Irrigation and Drainage Paper 56, FAO, Rome, Italy.

Allen, R. G., Walter, I. A., Elliot, R. L., Howell, T. A., Itenfisu, D., Jensen, M. E. & Snyder, R. 2005 *The ASCE standardized reference evapotranspiration equation*. American Society of Civil Engineers, Reston, VA.

Allen, R. G., Tasumi, M. & Trezza, R. 2007a Satellite-based energy balance for mapping evapotranspiration with internalized calibration, METRIC (model). *J. Irrig. Drain. Eng.* **133**, 380–394.

Allen, R., Tasumi, M., Morse, A., Trezza, R., Wright, J. L., Bastiaanssen, W., Kramber, W., Lorite, L. & Robison, C. W. 2007b Satellite-based energy balance for mapping evapotranspiration with internalized calibration, METRIC (applications). *J. Irrig. Drain. Eng.* **133**, 395–406.

Allen, R., Irmak, A., Trezza, R., Hendrickx, J. M. H., Bastiaanssen, W. G. M. & Kjaersgaard, J. 2011 Satellite-based ET estimation in agricultural using SEBAL and METRIC. *Hydrol. Process.* **25**, 4011–4027.

Bastiaanssen, W. G. M. 1995 Regionalization of surface flux densities and moisture indicators in composite terrain: a remote sensing approach under clear skies in Mediterrenean climates. PhD Dissertation, Koninklijke Bibliotheek, The Netherlands.

Bastiaanssen, W. G. M., Menenti, M., Feddes, R. A. & Holtslag, A. A. M. 1998a A remote sensing surface energy balance algorithm for land (SEBAL): 1. Formulation. *J. Hydrol.* **212–213**, 198–212.

Bastiaanssen, W. G. M., Pelgrum, H., Wang, J., Ma, Y., Moreno, J. F., Roerink, G. J. & van der Wal, T. 1998b A surface energy balance algorithm for land (SEBAL): 2. Validation. *J. Hydrol.* **212–213**, 213–229.

Baumgartner, A. & Reichel, E. 1975 *The World Water Balance*. Elsevier, Amsterdam, The Netherlands, p. 179.

Brutsaert, W. H. 1982 *Evaporation into the Atmosphere: Theory, History and Applications*. D. Reidel, Norwell, MA, USA.

Choi, M., Kustas, W. P., Anderson, M. C., Allen, R. G., Li, F. & Kjaaersgaard, J. H. 2009 An intercomparison of three remote sensing-based surface energy balance algorithms over a corn and soybean production region (Iowa, US) during SMACEX. *Agr. Forest Meteorol.* **149**, 2081–2097.

Choudhury, B. 1994 Synergism of multispectral satellite observations for estimating regional land surface evaporation. *Remote Sens. Environ.* **49**, 264–274.

Dingman, S. L. 1992 *Physical Hydrology*. Prentice Hall, Upper Saddle River, NJ, USA.

Gonzalez-Dugo, M. P., Neale, C. M. U., Mateos, L., Kustas, W. P., Prueger, J., Anderson, M. C. & Li, F. 2009 A comparison of operational remote-sensing-based models for estimating crop evapotranspiration. *Agr. Forest Meteorol.* **149**, 1843–1853.

Gowda, P. H., Chavez, J. L., Howell, T. A., Marek, T. H. & New, L. L. 2008 Surface energy balance based evapotranspiration mapping in the Texas high plains. *Sensors* **8**, 5186–5201.

Grindley, J. 1969 *The calculation of actual evapotranspiration and soil moisture deficit over specified catchment areas*. Hydrological Memorandum No. 38, Meteorological Office, Bracknell, UK.

Jia, L., Xi, G., Liu, S., Huang, C., Yan, Y. & Liu, G. 2009 Regional estimation of daily to annual regional evapotranspiration with MODIS data in the Yellow River Delta Wetland. *Hydrol. Earth Syst. Sci.* **13**, 1775–1787.

Liang, S. 2001 Narrowband to broadband conversion of land surface albedo. I. Formula, algorithms. *Remote Sens. Environ.* **76**, 213–238.

Menenti, M. & Choudhury, B. 1993 Parameterization of land surface evaporation by means of location dependent potential evaporation and surface temperature range. In: *Proceedings of IAHS Conference on Land Surface Processes*, IAHS, Wallingford, UK, 212, pp. 561–568.

Miralles, D. G., Holmes, T. R. H., De Jeu, R. A. M., Gash, J. H., Meesters, A. & Dolman, A. J. 2011 Global land-surface evaporation estimated from satellite-based observations. *Hydrol. Earth Syst. Sci.* **15**, 453–469.

Monteith, J. L. 1965 Evaporation and environment. In: *Proceedings of the 19th Symposium of the Society for Experimental Biology*. Cambridge University Press, New York, pp. 205–233.

Pastor, M. & Orgaz, F. 1994 Riego deficitario del olivar: los programas de recorte de riego en olivar. *Agricultura* **746**, 768–776.

Paul, G., Gowda, P. H., Varaprasad, P. V., Howell, T. A., Aiken, T. M., Hutchinson, S. L. & Neale, C. M. U. 2013 Role of hot and cold pixel concept in remote sensing based single source energy balance algorithms, using 21st century technology to better manage irrigation water supplies. In: *Seventh International Conference on Irrigation and Drainage*, Phoenix, AZ, USA.

Paul, G., Gowda, P. H., Varaprasad, P. V., Howell, T. A., Aiken, R. M. & Neale, C. M. 2014 Investigating the influence of roughness length for heat transport (zoh) on the performance of SEBAL in semi-arid irrigated and dryland agricultural systems. *J. Hydrol.* **509**, 231–244.

Penman, H. L. 1948 Natural evaporation from open water, bare soil and grass. *Proc. Roy. Soc. London* **A193**, 120–146.

Priestley, C. H. B. & Taylor, R. J. 1972 On the assessment of surface heat flux and evaporation using large-scale parameters. *Monthly Weather Review* **100**, 81–92.

Roerink, G. J., Su, Z. & Menenti, M. 2000 S-SEBI: a simple remote sensing algorithm to estimate the energy balance. *Phys. Chem. Earth* **25**, 147–157.

Singh, R. K. & Senay, G. B. 2016 Comparison of four different energy balance models for estimating evapotranspiration in the Midwestern United States. *Water* **8**, 9.

Su, Z. 2002 The surface energy balance system (SEBS) for estimation of turbulent heat fluxes. *Hydrol. Earth Syst. Sci.* **6**, 85–100.

Tasumi, M. 2003 Progress in operational estimation of regional evapotranspiration using satellite imagery. PhD Dissertation, University of Idaho, Moscow, ID, USA.

Tasumi, M., Allen, R. G., Trezza, R. & Wright, J. L. 2005 Satellite-based energy balance to assess within-population variance of crop coefficient curves. *J. Irrig. Drain. Eng.* **131** (1), 94–109.

Thornthwaite, C. W. 1948 An approach toward a rational classification of climate. *Geograph. Rev.* **38**, 55–94.

Thornthwaite, C. W. & Mather, J. R. 1955 *The Water Balance. Publications in Climatology*, Vol. VIII, No. 1. Drexel Institute of Technology, Centerton, NJ, USA.

Trenberth, K. E., Fasullo, J. T. & Kiehl, J. 2009 Earth's global energy budget. *Bull. Am. Meteor. Soc.* **87**, 597–606.

Turc, L. 1961 Evaluation des besoins en eau d'irrigation, evapotranspiration potentielle, formule climatique simplifice et mise a jour [Estimation of irrigation water requirements, evapotranspiration potential – a simple climatic formula evolved up to date]. *Ann. Agron.* **12**, 13–49.

Vinukollu, R. K., Wood, E. F., Ferguson, C. R. & Fisher, J. B. 2011 Global estimates of evapotranspiration for climate studies using multi-sensor remote sensing data: Evaluation of three process-based approaches. *Remote Sens. Environ.* **115**, 801–823.

WMO 2008 Guide to Hydrological Practices *(WMO No. 168)*, 8th edn. World Meteorological Organization, Geneva.

First received 3 November 2015; accepted in revised form 25 April 2016. Available online 3 June 2016